Journal of Alloys and Compounds 622 (2015) 925–928

Contents lists available at ScienceDirect

Journal of Alloys and Compounds

journal homepage: www.elsevier.com/locate/jalcom

Chemical stability and Ce doping of $LiMgAlF_6$ neutron scintillator

M.H. Du

Materials Science & Technology Division and Center for Radiation Detection Materials and Systems, Oak Ridge National Laboratory, Oak Ridge, TN 37831, USA

ARTICLE INFO

Article history:
Received 24 September 2014
Received in revised form 28 October 2014
Accepted 3 November 2014
Available online 13 November 2014

Keywords:
Neutron scintillator
$LiMgAlF_6$

ABSTRACT

Density functional calculations are performed to investigate $LiMgAlF_6$ as a potential neutron scintillator material. The calculations of enthalpy of formation and phase diagram show that single-phase $LiMgAlF_6$ can be grown but it should be more difficult than growing $LiCaAlF_6$ and $LiSrAlF_6$. The formation energy calculations for substitutional Ce show that the concentration of Ce on the Al site is negligible but a high concentration (>1 at.%) of Ce on the Mg site is attainable provided that the Fermi level is more than 5 eV lower than the conduction band minimum. Acceptor doping should promote Ce incorporation in $LiMgAlF_6$.

1. Introduction

$LiCaAlF_6$ (LiCAF) and $LiSrAlF_6$ (LiSAF) have been investigated as promising scintillator materials for neutron detection [1–20]. In particular, LiCAF has attracted considerable attention because (1) it has low atomic number and low density, which reduces sensitivity to background gamma rays; (2) its single crystals can be grown to large sizes using Czochralski growth methods [21]; and (3) it is not hygroscopic, which greatly simplifies material processing and application. The highest light yield reported for LiCAF:Eu^{2+} is 29,000 ph/n [10], which is higher than that of LiCAF:Ce^{3+}, which is currently 6600 ph/n [1]. Pulse shape discrimination between neutron and gamma ray has been demonstrated for LiCAF:Ce^{3+} [13].

Despite the significant progress made in LiCAF scincillators in the last decade, there are only a few studies carried out on $LiMgAlF_6$ (LiMAF) [22–24], which has lower atomic number than LiCAF and therefore is less sensitive to background gamma-rays than LiCAF. LiMAF has a hexagonal structure (space group P321, No. 150) [25]. This is different from LiCAF and LiSAF, which belong to a large family of minerals known as colquiriites (space group P-31c, No. 163) [26]. No large single crystal growth of LiMAF has been reported. However, the growth of the single-phase LiMAF has been demonstrated [22–24]. Luminescence in Ce and Eu doped LiMAF has been reported [22,23]. The emission of LiMAF: Ce^{3+} has one broad band centered at 330 nm [23]. It should be noted that CeF_3 has a similar broad-band emission centered at 340 nm [27,28]. Since obtaining single-phase LiMAF is relatively difficult [22–24], it is important to verify whether a high Ce concentration in LiMAF can be attained without forming CeF_3 phase. For Eu doped LiMAF, emission bands centered at 370 nm [22,24] and 593 nm [23,24] have been reported for LiMAF samples prepared by using different methods. The 370-nm and 593-nm emission bands were attributed to emissions from Eu^{2+} and Eu^{3+}, respectively.

Availability of large single crystals is critically important for the development of the scintillator materials. The chemical stability of the compound is important for the growth of large single crystals. In this paper, we show the calculated enthalpy of formation for LiMAF and compare it to those of LiCAF and LiSAF. The phase diagram of LiMAF is also calculated. In addition, we have performed calculations to understand the origin of the Ce emission and the viability of Ce as an effective activator in $LiMgAlF_6$. The important questions that we address in this work include whether the emission is from Ce on Mg or Al site in $LiMgAlF_6$ and whether a high Ce concentration is attainable in LiMAF. These are the critical issues that need to be resolved for the development of LiMAF as a potential neutron scintillator material.

2. Methods

Density functional calculations were performed to study the chemical stability and Ce doping in LiMAF [29]. Perdew–Burke–Ernzerhof (PBE) [30] exchange–correlation functionals were used to calculate enthalpy of formation for LiMAF, LiCAF, and LiSAF. Hybrid functionals [31], which employ 38.5% of Fock exchange [16], were also used to calculate enthalpy of formation, phase diagram, and formation energies of Ce dopant in LiMAF. The hybrid functional calculations, which can partially remove the self-interaction error and correct the band gap, have recently been applied to defect calculations and have generally shown improvement in structural, electronic, dielectric, and defect properties in semiconductors [32–40]. The calculated band gap of LiCAF is 12.63 eV using hybrid functional, close to the experimental value of 12.65 eV [41]. Using the same method, the band gap of LiMAF is calculated to be 12.78 eV. (No experimental result is available for the band gap of LiMAF.) The electron–ion interactions were described using projector augmented wave potentials [42]. The valence wavefunctions were expanded in a plane-wave

http://dx.doi.org/10.1016/j.jallcom.2014.11.022
0925-8388/

basis with a cutoff energy of 500 eV. All the calculations were performed using a 54-atom supercell containing six formula units of LiMAF. A $2 \times 2 \times 2$ grid was used for the k-point sampling of Brillouin zone. Feynman–Hellmann forces were minimized to below 0.05 eV/Å in structural relaxation calculations.

The defect formation energy is given by

$$\Delta H = \Delta E - \sum_i n_i \left(\mu_i + \mu_i^{ref}\right) + q(\varepsilon_{VBM} + \varepsilon_f), \quad (1)$$

where ΔE is the energy difference between the defect-containing and defect-free supercells, and n_i is the difference in the number of atoms for the ith atomic species between the defect-containing and defect-free supercells. μ_i is the relative chemical potential for the ith atomic species, referenced to μ_i^{ref}. For Li, Mg, Al, Ce, and F, μ_{Li}^{ref}, μ_{Mg}^{ref}, μ_{Al}^{ref}, μ_{Ce}^{ref}, and μ_F^{ref} are metallic Li, Mg, Al, and Ce, and half of the total energy of the gas-phase F_2 molecule, respectively. ε_f is the Fermi energy referenced to the valance band maximum (VBM), ε_{VBM}. The thermal-equilibrium defect concentration is given by

$$N = N_0 \exp(-\Delta H/kT) \quad (2)$$

where N_0 is the number of available lattice sites for defect formation, k is the Boltzmann constant, and T is the temperature.

3. Results and discussion

3.1. Chemical stability of LiMAF, LiCAF, and LiSAF

Reactions of binary metal fluorides to form quaternary LiMAF, LiCAF, and LiSAF are all exothermic. The following are the reaction energies for LiMAF, LiCAF, and LiSAF, calculated using PBE functionals:

$$LiF + MgF_2 + AlF_3 \xrightarrow{-0.18\ eV} LiMgAlF_6,$$

$$LiF + CaF_2 + AlF_3 \xrightarrow{-0.36\ eV} LiCaAlF_6,$$

$$LiF + SrF_2 + AlF_3 \xrightarrow{-0.39\ eV} LiSrAlF_6.$$

The reaction energy for LiMAF is also calculated by using hybrid functionals, which yields −0.17 eV, close to the PBE result. One can see that LiMAF is least stable against decomposition to binary phases. This is consistent with the experimental observation of the difficulty in growing single-phase LiMAF [22–24].

3.2. Phase diagram of LiMAF

Phase diagram of LiMAF is calculated using hybrid functional calculations. Stability of the single-phase LiMAF requires no spontaneous formation of the following phases: metallic Li, Mg, and Al, F_2 gas, and binary LiF, MgF_2, and AlF_3. Therefore, the following conditions should be met:

$$\mu_{Li} + \mu_{Mg} + \mu_{Al} + 6\mu_F = \Delta H(LiMgAlF_6) = -33.447\ eV, \quad (3)$$

$$\mu_{Li} + \mu_F \le \Delta H(LiF) = -6.326\ eV, \quad (4)$$

$$\mu_{Mg} + 2\mu_F \le \Delta H(MgF_2) = -11.484\ eV, \quad (5)$$

$$\mu_{Al} + 3\mu_F \le \Delta H(AlF_3) = -15.467\ eV, \quad (6)$$

$$\mu_{Li} \le 0, \quad (7)$$

$$\mu_{Mg} \le 0, \quad (8)$$

$$\mu_{Al} \le 0, \quad (9)$$

$$\text{and} \quad \mu_F \le 0, \quad (10)$$

where $\Delta H(LiMgAlF_6)$, $\Delta H(LiF)$, $\Delta H(MgF_2)$, and $\Delta H(AlF_3)$ are the enthalpy of formation for LiMAF, LiF, MgF_2, and AlF_3, respectively. The four variables (μ_{Li}, μ_{Mg}, μ_{Al}, and μ_F) can be reduced to three by combining Eq. (3) with Eqs. (4-6):

$$5\mu_{Li} - \mu_{Mg} - \mu_{Al} \le -4.510\ eV, \quad (11)$$

$$-\mu_{Li} + 2\mu_{Mg} - \mu_{Al} \le -1.005\ eV, \quad (12)$$

$$-\mu_{Li} - \mu_{Mg} + \mu_{Al} \le 2.513\ eV. \quad (13)$$

Combining Eqs. (3) and (10), one obtains

$$\mu_{Li} + \mu_{Mg} + \mu_{Al} \le -33.447\ eV \quad (14)$$

Eqs. (7)–(9), (11)–(14) determine the phase diagram of LiMAF, which is shown in Fig. 1. The three planes (Eqs. (11)–(13)) that define the phase boundaries of the three binary compounds (LiF, MgF_2, and AlF_3) are drawn in Fig. 1 (magenta, cyan, and green planes, respectively). Eqs. (7)–(9) define Li, Mg, and Al rich limits, respectively, which correspond to $\mu_{Li} = 0$, $\mu_{Mg} = 0$, and $\mu_{Al} = 0$ planes in Fig. 1. The F-rich limit, $\mu_F = 0$ or $\mu_{Li} + \mu_{Mg} + \mu_{Al} = -33.447$ eV (Eq. (14)), is shown by the yellow plane in Fig. 1. The stability region of LiMAF is a narrow triangular prism confined by five planes in Fig. 1, i.e., the three planes that define the phase boundaries of LiF, MgF_2, and AlF_3 (magenta, cyan, and green planes, respectively) and the F-rich (yellow plane) and Al-rich ($\mu_{Al} = 0$ plane) planes. The LiMAF stability region (a triangular prism) shown in Fig. 1(a) and (b) is behind and in front of the yellow plane in the figure, respectively. Fig. 1(c) shows the zoom-in image of the triangular prism inside the black rectangle in Fig. 1(b). It can be seen that the stability region of LiMAF in the phase diagram is very small and is very close to the phase spaces for the three binary compounds. The intersection between the triangular prism and the Al-rich plane ($\mu_{Al} = 0$ plane) is a triangle with three side lengths of only 0.24, 0.25, and 0.29 eV. These results show that the growth of single-phase LiMAF requires careful control of stoichiometry to avoid binary phase segregation.

3.3. Formation energies of substitutional Ce

Formation energies of substitutional Ce on both Al and Mg sites are calculated using hybrid functionals. Ce^{3+} is isovalent to Al^{3+} in LiMAF. Following Eq. (1), the formation energy of neutral Ce_{Al}^0 is calculated to be

$$\Delta H\left(Ce_{Al}^0\right) = 0.004\ eV - \mu_{Ce} + \mu_{Al}, \quad (15)$$

where μ_{Ce} and μ_{Al} are chemical potentials of Ce and Al in LiMAF, respectively, relative to those of their metallic phases. Eq. (15) can be rewritten to $\Delta H\left(Ce_{Al}^0\right) = 0.004\ eV - \mu_{Ce} - 3\mu_F + \mu_{Al} + 3\mu_F$. The LiMAF phase diagram in Fig. 1 shows that the stable region for LiMAF is very close to the binary phase spaces. Therefore, $\mu_{Al} + 3\mu_F \approx \Delta H(AlF_3)$, where $\Delta H(AlF_3)$ is the enthalpy of formation for AlF_3. Assuming Ce-rich limit, $\mu_{Ce} + 3\mu_F = \Delta H(CeF_3)$, where $\Delta H(CeF_3)$ is the enthalpy of formation for CeF_3. Using calculated heats of formation, i.e., $\Delta H(AlF_3) = -15.467$ eV and $\Delta H(CeF_3) = -18.255$ eV, Eq. (15) can be approximated to

$$\Delta H\left(Ce_{Al}^0\right) = 0.004\ eV - \Delta H(CeF_3) + \Delta H(AlF_3) = 2.79\ eV. \quad (16)$$

Eq. (16) shows that, even at the Ce-rich limit, the formation energy of Ce_{Al}^0 is too high to allow a high concentration of Ce_{Al}^0 in LiMAF. Using Eq. (2) and the growth temperature of 1008 K [23], the Ce_{Al}^0 concentration is only $1.17 \times 10^8\ cm^{-3}$ at the Ce-rich limit. Therefore, the concentration of Ce_{Al}^0 in LiMAF is negligible.

Ce^{3+} can also occupy the Mg^{2+} site, acting as a single electron donor, Ce_{Mg}^+. Following Eq. (1), one obtains the formation energy of Ce_{Mg}^+:

$$\Delta H\left(Ce_{Mg}^+\right) = -8.95\ eV - \mu_{Ce} + \mu_{Mg} + \varepsilon_f \quad (17)$$

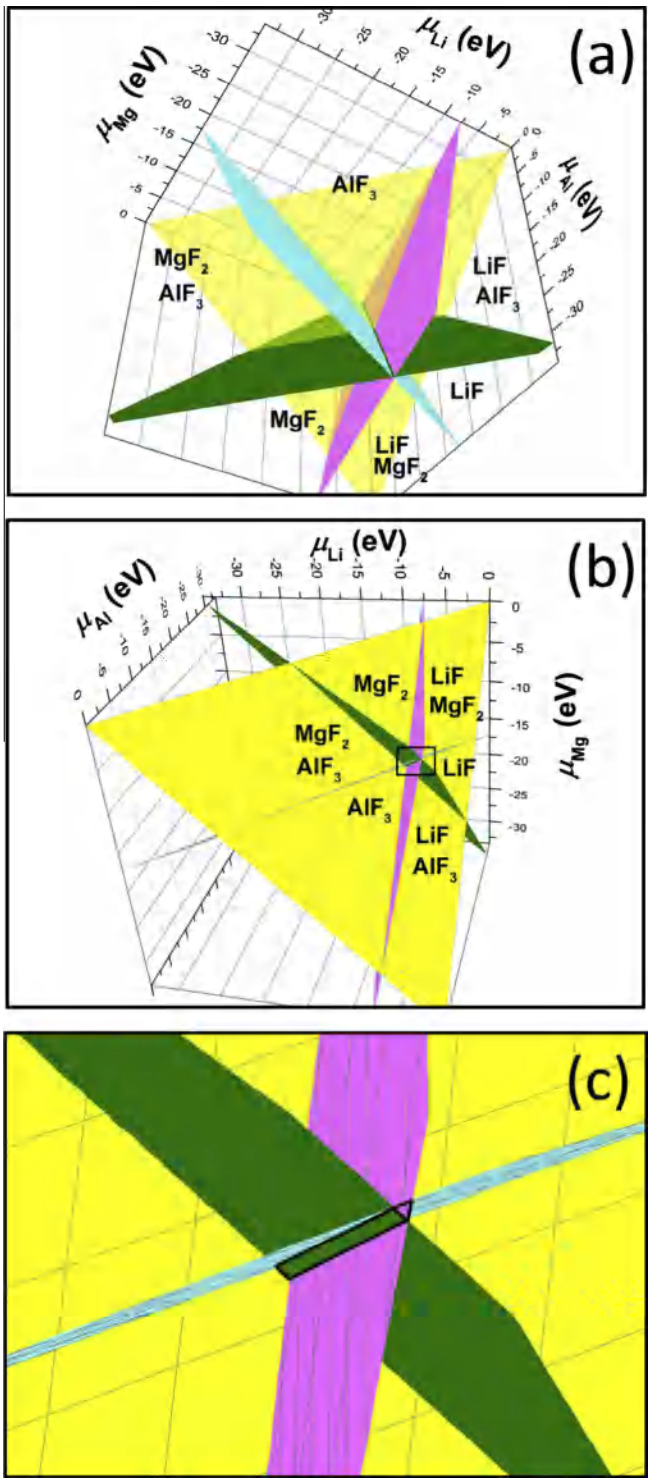

Fig. 1. Phase diagram of LiMAF. The stability region for LiMAF is a narrow triangular prism behind and in front of the yellow plane in (a) and (b). (c) shows the zoom-in image of the triangular prism in the black rectangle in (b). (For interpretation of the references to color in this figure legend, the reader is referred to the web version of this article.)

where μ_{Mg} is the chemical potential of Mg in LiMAF relative to that of metallic bulk Mg and ε_f is the Fermi level relative to the VBM. Due to the proximity of the LiMAF phase to MgF_2 phase in the phase diagram (Fig. 1), $\mu_{Mg} + 2\mu_F \approx \Delta H(MgF_2)$, where $\Delta H(MgF_2)$ is the enthalpy of formation for MgF_2. Assuming Ce-rich limit, $\mu_{Ce} + 3\mu_F = \Delta H(CeF_3)$. Using calculated heats of formation, i.e., $\Delta H(MgF_2) = -11.484$ eV and $\Delta H(CeF_3) = -18.255$ eV, Eq. (17) can be approximated to

$$\Delta H\left(Ce^{+}_{Mg}\right) = -8.95 \text{ eV} - \Delta H(CeF_3) + \Delta H(MgF_2) + \mu_F + \varepsilon_f$$
$$= -2.18 \text{ eV} + \mu_F + \varepsilon_f \quad (18)$$

At the F-poor limit (lowest μ_F, where the magenta and cyan planes intersect with the $\mu_{Al} = 0$ plane), $\mu_F = -5.212$ eV. Thus, one obtains

$$\Delta H\left(Ce^{+}_{Mg}\right) \geq -7.39 \text{ eV} + \varepsilon_f \quad (19)$$

Using Eqs. (2) and (19), it can be shown that, to obtain 1 at.% of Ce^{+}_{Mg} in LiMAF at 1008 K, the maximum Fermi level is 7.79 eV above the VBM ($\varepsilon_f = 7.79$ eV), which is about 5 eV below the conduction band minimum (the calculated band gap is 12.78 eV). This is calculated under the conditions of Ce-rich and F-poor limits. These results show that it is possible to obtain a high concentration of Ce^{+}_{Mg}. Note that Ce concentrations above 1 at.% have been demonstrated in both LiCAF and LiSAF [11,19]. Since low Fermi level promotes the formation of Ce^{+}_{Mg}, acceptor doping in LiMAF is desirable to obtain high Ce concentration.

4. Conclusions

Density functional calculations show that LiMAF is more prone to decomposition to binary phases than LiCAF and LiSAF. The calculated phase diagram shows a small stability region for single-phase LiMAF. These results suggest that the single-phase LiMAF can be grown but requires careful control of stoichiometry to avoid segregation of binary phases. The formation energy calculations of substitutional Ce on both Al and Mg sites show that the concentration of Ce^{0}_{Al} is negligible whereas a high concentration (i.e., >1 at.%) of Ce^{+}_{Mg} is attainable provided that the Fermi level is more than 5 eV below the conduction band minimum. Therefore, acceptor doping in LiMAF is desirable to increase the Ce concentration in LiMAF.

Acknowledgements

The author is grateful for helpful discussion with David J. Singh. The work was supported by the U.S. DOE Office of Nonproliferation Research and Development NA22.

References

[1] M. Nikl, N. Solovieva, E. Mihokova, M. Dusek, A. Vedda, M. Martini, K. Shimamura, T. Fukuda, Phys. Status Solidi A 187 (2001) R1.
[2] A. Gektin, N. Shiran, S. Neicheva, V. Gavrilyuk, A. Bensalah, T. Fukuda, K. Shimamura, Nucl. Instrum. Methods Phys. Res., A 486 (2002) 274.
[3] A.V. Gektin, N.V. Shiran, S.V. Neicheva, M.J. Weber, S.E. Derenzo, W.W. Moses, J. Lumin. 102–103 (2003) 460.
[4] N. Shiran, A. Gektin, S. Neicheva, M. Weber, S. Derenzo, M. Kirm, M. True, I. Shpinkov, D. Spassky, K. Shimamura, N. Ichinose, Nucl. Instrum. Methods Phys. Res., A 537 (2005) 266.
[5] S. Neicheva, A. Gektin, N. Shiran, K. Shimamura, E. Villora, Radiat. Meas. 42 (2007) 811.
[6] A. Yoshikawa, T. Yanagida, Y. Yokota, N. Kawaguchi, S. Ishizu, K. Fukuda, T. Suyama, K.J. Im, J. Pejchal, M. Nikl, K. Watanabe, M. Miyake, M. Babam, K. Kamada, IEEE Trans. Nucl. Sci. 56 (2009) 3796.
[7] T. Yanagida, A. Yoshikawa, Y. Yokota, S. Maeo, N. Kawaguchi, S. Ishizu, K. Fukuda, T. Suyama, Opt. Mater. 32 (2009) 311.
[8] J. Pejchal, E. Mihokova, M. Nikl, A. Novoselov, A. Yoshikawa, Opt. Mater. 31 (2009) 1673.
[9] A. Yoshikawa, T. Yanagida, Y. Yokota, A. Yamaji, Y. Fujimoto, J. Pejchal, V.I. Chani, N. Kawaguchi, S. Ishizu, K. Fukuda, T. Suyama, M. Nikl, Opt. Mater. 32 (2010) 845.
[10] T. Yanagida, N. Kawaguchi, Y. Fujimoto, K. Fukuda, Y. Yokota, A. Yamazaki, K. Watanabe, J. Pejchal, A. Uritani, T. Iguchi, A. Yoshikawa, Opt. Mater. 33 (2011) 1243.
[11] Y. Yokota, Y. Fujimoto, T. Yanagida, H. Takahashi, M. Yonetani, K. Hayashi, I. Park, N. Kawaguchi, K. Fukuda, A. Yamaji, Y. Fukazawa, M. Nikl, A. Yoshikawa, Cryst. Growth Des. 11 (2011) 4775.

[12] N. Kawaguchi, T. Yanagida, Y. Fujimoto, Y. Yokata, K. Kamada, K. Fukuda, T. Suyama, K. Watanabe, A. Yamazaki, V. Chani, A. Yoshikawa, Nucl. Instrum. Methods Phys. Res., A 652 (2011) 351.
[13] A. Yamazaki, K. Watanabe, A. Uritani, T. Iguchi, N. Kawaguchi, T. Yanagida, Y. Fujimoto, Y. Yokata, K. Kamada, K. Fukuda, T. Suyama, A. Yoshikawa, Nucl. Instrum. Methods Phys. Res., A 652 (2011) 435.
[14] J. Iwanowska, L. Swiderski, M. Moszynski, T. Yanagida, Y. Yokata, A. Yoshikawa, K. Fukuda, N. Kawaguchi, S. Ishizu, Nucl. Instrum. Methods Phys. Res., A 652 (2011) 319.
[15] N.V. Shiran, A.V. Gektin, S.V. Neicheva, V.A. Kornienko, K. Shimamura, N. Ishinose, J. Lumin. 102–103 (2003) 815.
[16] M.H. Du, D.J. Singh, J. Appl. Phys. 112 (2012) 123516.
[17] M. Koshimizu, T. Yanagida, Y. Fujimoto, A. Yamazaki, K. Watanabe, A. Uritani, K. Fukuda, N. Kawaguchi, S. Kishimoto, K. Asai, Appl. Phys. Express 6 (2013) 062601.
[18] M. Nikl, P. Bruza, D. Panek, M. Vrbova, E. Mihokova, J.A. Mares, A. Beitlerova, N. Kawaguchi, K. Fukuda, A. Yoshikawa, Appl. Phys. Lett. 102 (2013) 161907.
[19] A. Yamaji, T. Yanagida, N. Kawaguchi, Y. Fujimoto, Y. Yokota, K. Watanabe, A. Yamazaki, A. Yoshikawa, J. Pejchal, Nucl. Instrum. Methods Phys. Res., A 659 (2011) 368.
[20] A. Yamaji, Y. Yokota, T. Yanagida, N. Kawaguchi, Y. Futami, Y. Fjimoto, A. Yoshikawa, J. Cryst. Growth 352 (2012) 106.
[21] K. Shimamura, H. Sato, A. Bensalah, H. Machida, N. Sarukura, T. Fukuda, J. Alloys Comp. 343 (2002) 204.
[22] P.D. Belsare, C.P. Joshi, S.V. Moharil, S.K. Omanwar, P.I. Muthal, S.M. Dhopte, J. Lumin. 129 (2009) 135.
[23] F. Tao, X. Zhou, S. Zhu, B. Zhao, G. Hong, H. You, Cryst. Res. Technol. 32 (1997) 849.
[24] F. Tao, G. Hong, S. Zhu, H. You, X. Zhou, B. Zhao, Phys. Status Solidi A 165 (1998) 303.
[25] P. Villars, K. Cenzual, Pearson's Crystal Data: Crystal Structure Database for Inorganic Compounds (on DVD), Release 2012/13, ASM International®, Materials Park, Ohio, USA, 2012.
[26] S. Kuze, D. du Boulay, N. Ishizawa, N. Kodama, M. Yamaga, B. Henderson, J. Solid State Chem. 177 (2004) 3505.
[27] D.F. Anderson, IEEE Trans. Nucl. Sci. 36 (1989) 137.
[28] W.W. Moses, S.E. Derenzo, IEEE Trans. Nucl. Sci. 36 (1989) 173.
[29] G. Kresse, J. Furthmüller, Phys. Rev. B 54 (1996) 11169.
[30] J.P. Perdew, K. Burke, M. Ernzerhof, Phys. Rev. Lett. 77 (1996) 3865.
[31] J.P. Perdew, M. Ernzerhof, K. Burke, J. Chem. Phys. 105 (1996) 9982.
[32] J. Paier, M. Marsman, K. Hummer, G. Kresse, I.C. Gerber, J.G. Angyan, J. Chem. Phys. 124 (2006) 154709.
[33] D. Muñoz Ramo, A.L. Shluger, J.L. Gavartin, G. Bersuker, Phys. Rev. Lett. 99 (2007) 155504.
[34] D. Muñoz Ramo, J.L. Gavartin, A.L. Shluger, G. Bersuker, Phys. Rev. B 75 (2007) 205336.
[35] A. Alkauskas, P. Broqvist, A. Pasquarello, Phys. Rev. Lett. 101 (2008) 046405.
[36] A. Alkauskas, P. Broqvist, F. Devynck, A. Pasquarello, Phys. Rev. Lett. 101 (2008) 106802.
[37] M.H. Du, S.B. Zhang, Phys. Rev. B 80 (2009) 115217.
[38] A. Janotti, J.B. Varley, P. Rinke, N. Umezawa, G. Kresse, C.G. Van de Walle, Phys. Rev. B 81 (2010) 085212.
[39] K. Biswas, M.H. Du, Appl. Phys. Lett. 98 (2011) 181913.
[40] H.-P. Komsa, P. Broqvist, A. Pasquarello, Phys. Rev. B 81 (2010) 205118.
[41] M. Kirm, M. True, S. Vielhauer, G. Zimmerer, N.V. Shiran, I. Shpinkov, D. Spassky, K. Shimamura, N. Ichinose, Nucl. Instrum. Methods Phys. Res., A 537 (2005) 291.
[42] G. Kresse, D. Joubert, Phys. Rev. B 59 (1999) 1758.